Density Functional Theory and Experimental Determination of Band Gaps and lattice parameters in Kesterite $Cu_2ZnSn(S_xSe_{1-x})_4$

Chuan-Jia Tong*[1], Holly J. Edwards[2], Theodore D. C. Hobson[2], Ken Durose[2], Vinod R. Dhanak[2], Jonathan D. Major[2], Keith P. McKenna[1]

1. *Department of Physics, University of York, Heslington, York, YO10 5DD, UK*
2. *Stephenson Institute for Renewable Energy, Department of Physics, University of Liverpool, Liverpool, L69 7ZF, UK*

*Email: chuanjia.tong@york.ac.uk

ABSTRACT

The structures and band gaps of copper-zinc-tin-selenosulfides (CZTSSe) are investigated for a range of anion compositions through experimental analysis and complementary first-principles simulations. The band gap is found to be extremely sensitive to the Sn-anion bond length, with an almost linear correlation with the average Sn-anion bond length in the mixed anion phase $Cu_2ZnSn(S_xSe_{1-x})_4$. Therefore, accurate prediction of band gaps using first principles methods requires accurate reproduction of the experimental bond lengths. This is challenging for many widely used approaches that are suitable for large supercells. The HSE06 functional is found to predict structure and band gap in good agreement with experiment but is computationally expensive for large supercells. It is shown that geometry optimization with the MS2 meta-GGA functional followed by single point calculation of electronic properties using HSE06 is a reasonable compromise for modelling larger supercells that are often unavoidable in the study of point and extended defects.

TOC:
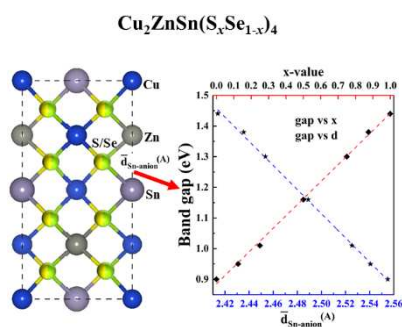
The quaternary compound semiconductors Cu_2ZnSnS_4 (CZTS) and $Cu_2ZnSnSe_4$ (CZTSe) show exceptional promise as low-cost and sustainable solar absorbers for next generation thin-film photovoltaic cells. They have direct band gaps in the range 1 to 1.5 eV, exhibit strong optical absorption and unlike many of the alternative materials all of the constituent elements are non-toxic and earth abundant.[1-5] Following the first report of kesterite CZTS solar cells with 0.66%[6] solar conversion efficiency, decades of research have led to significant improvements in efficiency (now at 12.6%[7]). This improvement in performance has required careful control over stoichiometry to minimize harmful intrinsic defects such as vacancies (V_{Cu}, V_{Zn}), antisite defects (Zu_{Cu}, Cu_{Sn}) and defect-complexes ($V_{Cu}+Zn_{Cu}$) as well as the formation of unwanted secondary phases.[8-11] Recent work is beginning to explore mixed anion phases[12-18], i.e. $Cu_2ZnSn(S_xSe_{1-x})_4$ (CZTSSe), to enable tuning of the band gap and further enhancement of efficiency and an almost linear relationship between the band gap and x has been found.[19-20] CZTS and CZTSe have quite different lattice constants and as a result many bond lengths change as one varies x (which will affect both band positions and widths). On the other hand, although isovalent S and Se are similar chemically changes in the orbital character of bands cannot be excluded either. First principles calculations[21-25] have been employed to investigate both pure and mixed anion phases of CZTS and CZTSe, however an issue that has often been overlooked is that common approaches (e.g. structural optimization using DFT with GGA approximations to exchange and correlation followed by calculation of electronic properties using hybrid functionals) yield significant errors in structures and band gaps. Therefore, a detailed investigation into the effects of anion mixing on structure and band gaps including validation against experiment is very much needed to provide a solid foundation for future materials optimization.

In this letter, we report first-principles calculations of the structure and electronic properties of CZTSSe mixed anion phases as well as the pure end phases which we compare to experimental data for both thin film and bulk crystalline samples. Our results highlight the fact that Sn-S/Se bonds play a vital role in determining the band gap of this kesterite material. Moreover, it is the average Sn-anion bond length that determines the linear relationship between band gap and the mixing parameter x in $Cu_2ZnSn(S_xSe_{1-x})_4$. Our work not only clarifies the atomistic mechanism behind the linear band gap behavior in CZTSSe, but also highlights the fact that care should be taken to closely reproduce the experimental structure of these materials. It is essential to find computationally inexpensive methods that can predict structure accurately to enable accurate simulation of defects that require large supercells (such as point defects, surfaces or grain boundaries). We show that the meta-GGA functional MS2 is superior to traditional GGA methods in this regard.

Figure 1 shows the calculated band gaps of CZTS and CZTSe for both equilibrium and isotropically strained crystals (within the range +/- 5%) using the HSE06 hybrid functional. We obtain excellent

agreement with experiment for both the equilibrium lattice constants and band gaps (both differ by less than 1.5%, as shown in Figure 2a). For the strained crystals, we also predict an almost linear correlation between the calculated band gap and the Sn-anion bond length (dashed lines in Figure 1). Importantly, the band bap is very sensitive to this bond length with a ~0.1 Å change giving rise to more than 0.5 (0.4) eV change in the band gap of CZTS (CZTSe). This strong sensitivity was also noted in recent study by Ji-Sang Park et al.[26] Importantly, we note that if one optimizes the structure of CZTS or CZTSe using the PBE exchange-correlation functional (triangles in Figure 1), the lattice constants and Sn-anion bond length are significantly overestimated (equivalent to an expansive strain of around 5%). Along with the variation in lattice constants, the Sn-S and Sn-Se bond lengths also vary with x. Importantly, even exchange correlation approximations that yield similar lattice constants can have significant differences in the Sn-S and Sn-Se bond lengths that affect prediction of band gaps (Figure S1 in SI). As a result, if one then performs a single point calculation using HSE06 to calculate the band gap (a common approach especially for large supercells where full optimization at the hybrid level is prohibitively expensive), it will be significantly underestimated. To allow more reliable comparison to experimental data all subsequent results for the mixed phases were obtained using full optimization at the HSE06 level.
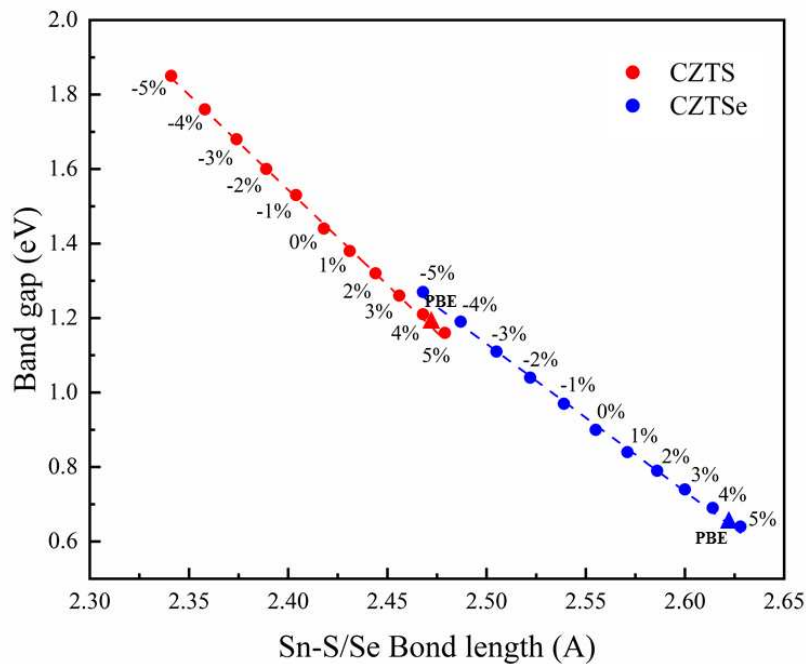
Figure 1. Band gaps for CZTS and CZTSe calculated using the HSE06 functional for the equilibrium and isotropically strained crystals (in all cases internal parameters are fully optimized). The dashed lines show the linear fit between band gap and the Sn-S or Sn-Se bond length. Also shown is the result of a full structural optimization using the PBE exchange-correlation functional followed by single point calculation of band gap with HSE06 (triangles).

In the mixed anion phase, where Sn-S and S-Se bonds with a distribution of lengths may be present, it remains an open question how the variation of the band gap with composition depends on internal parameters. To address this question we compute the structure and band gap of a series of mixed anion phases with $x=$ 0, 1/8, 1/4, 1/2, 3/4, 7/8 and 1. For each x, all possible anion configurations are considered and then full lattice optimizations are carried out (see details in Figure S2 in SI). The most stable anion configuration is used for subsequent analysis however we find there is little difference in total energy, structure and electronic properties for different anion configurations. Figure 2a shows how the calculated lattice constants of $Cu_2ZnSn(S_xSe_{1-x})$ vary with x. For comparison, we consider the lattice constants determined by Rietveld refinement for two different types of experimental sample: bulk crystallised samples fabricated via solution growth and thin film samples prepared by spray pyrolysis ('Crystal' and 'Thin film' in Figure 2, respectively). Full details are given in the Methods section. The lattice constants are found to vary linearly between the end points and there is a very good agreement between the theoretical predictions and experimental data (differing by less than 1.5% for the 'Crystal' samples). More details can be seen in Tables S1, S2 and S3 in SI.

For the analysis of bond lengths in $CZT(S_xSe_{1-x})_4$ we define an effective average Sn-anion bond length in the following way,

$$\bar{d}_{Sn-anion} = \frac{\sum_{i=1}^{N_{Sn-S}} d_{Sn-S}^i + \sum_{i=1}^{N_{Sn-Se}} d_{Sn-Se}^i}{N_{Sn-S} + N_{Sn-Se}} \tag{1}$$

where d_{Sn-S} and d_{Sn-Se} are the bond lengths of Sn-S and Sn-Se in $CZT(S_xSe_{1-x})_4$, and N_{Sn-S} (N_{Sn-Se}) are the number of Sn-S (Sn-Se) bonds in the supercell, thus their summary equals to the number of Sn-anion bonds $N_{Sn-anion}$. Namely, $N_{Sn-S} = xN_{Sn-anion}$. For comparison, the average bond lengths are also determined for the bulk crystalline samples by Rietveld refinement (assuming Sn atoms occupy fixed positions in the unit cell and considering S and Se sites as identical to one another). While we were able to produce consistent lattice parameters for the thin films, we note that it was not possible to determine reliable average bond lengths. This was due to inaccuracies with the anion positions after the refinement which was most likely caused by the preferred orientation of the thin films. As expected, the predicted and experimental average bond lengths are found to vary in a highly linear manner with x (Figure 2b). There is very close agreement between the predicted and experimental average bond length for the pure CZTSe phase ($x = 0$). However, a larger difference is found in pure CZTS ($x = 1$), which in previous work we attributed to stronger Cu-Zn disorder in CZTS compared to CZTSe which affects unit cell volume, vibrational mode frequencies and bond lengths[27]. For each mixed phase we also compute the band gap and compare against the experimental optical gap obtained via Tauc plots for the 'Thin film' samples (right scale of Figure 2b). Once again, we find good agreement both in terms of the linear trend and absolute band gaps (to within ~0.1 eV) across the entire range, agreeing well with previous reports.
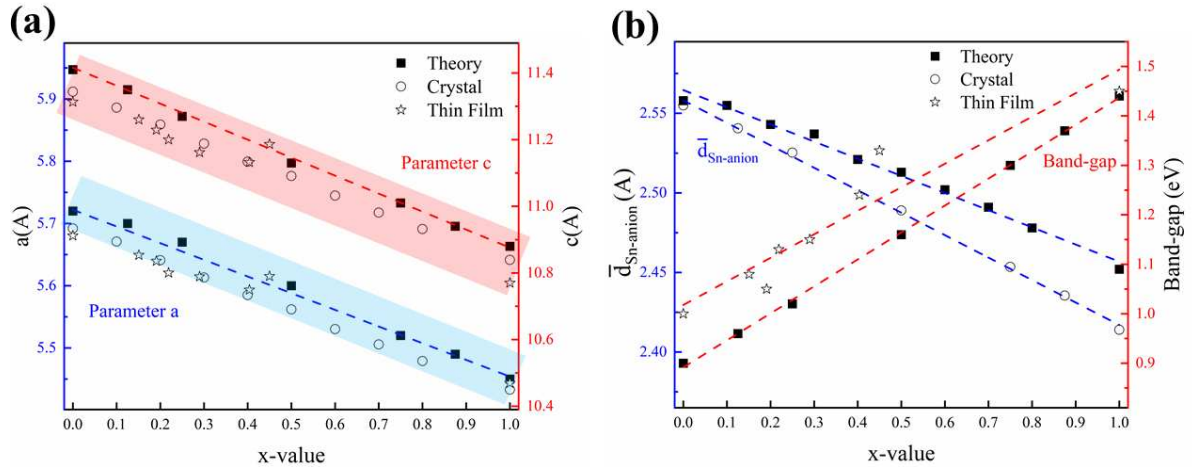
Figure 2. (a) Theoretical (solid square) and experimental (open circle: salt crystallised samples; open star: thin film samples) lattice constants a (left scale, blue) and c (right scale, red) for CZT(S$_x$Se$_{1-x}$)$_4$. (b) Variation of the average Sn-anion bond length (left scale, blue) and band gap (right scale, red) with x. Dashed lines show linear fits to the data. The HSE06 functional is used throughout both structural optimization and band gap calculation.

These results suggest HSE06 is a reliable (albeit computationally expensive) approach for predicting the structure and band gaps of CZT(S$_x$Se$_{1-x}$)$_4$. To illustrate the effect of employing different XC we also compute properties of the anion mixed phases employing PBE and MS2 (a meta-GGA functional) for geometry optimization followed by single point calculation of band gaps with HSE06 (Figure S1 in SI). In all cases we find that the average bond length varies in a highly linear manner with x in the mixing phase. However, average bonds lengths obtained using PBE are highly overestimated leading to highly underestimated band gaps. On the other hand, MS2 predicts very similar structural properties to HSE06 hence HSE06@MS2 (i.e. HSE06 calculation of electronic properties at the MS2 geometry) gives very similar electronic properties to fully self-consistent HSE06 (see Table S4 in SI). Moreover, the computational cost of MS2 is only 1.3~1.5 times that of PBE, whereas it is over 1000 times the cost for HSE06. Therefore, this approach should be computationally efficient yet accurate for simulations requiring large supercells in CZTS/Se.

Figure 3a shows that the variation of band gap with x (red dashed line) for CZT(S$_x$Se$_{1-x}$)$_4$ is highly linear, correlating strongly with average Sn-anion bond length. The conduction band minimum (CBM) in pure CZTS (CZTSe) phase is derived from Sn-S (Se) antibonding states as shown in Densities of states (DOS) in Figure 3b. Figure 3c shows a charge density isosurface for the CBM when x equals to 0.5, indicating that it involves antibonding between the Sn-5s and S-3p as well as Sn-5s and Se-4p orbitals when combining with DOS. On mixing the nature of the conduction band minimum state does

not change significantly. However, the increase in bond length caused by the larger Se ion weakens the antibonding interaction and therefore lowers the conduction band minimum (see Figure 3d for a schematic). The valence band maximum which has Cu-anion character does not change significantly with x. Similar results are obtained for all other anion compositions, confirming that the linear band gap behavior in the mixed anion phases is determined by the shift of CBM induced by changes in Sn-S/Se bond lengths.
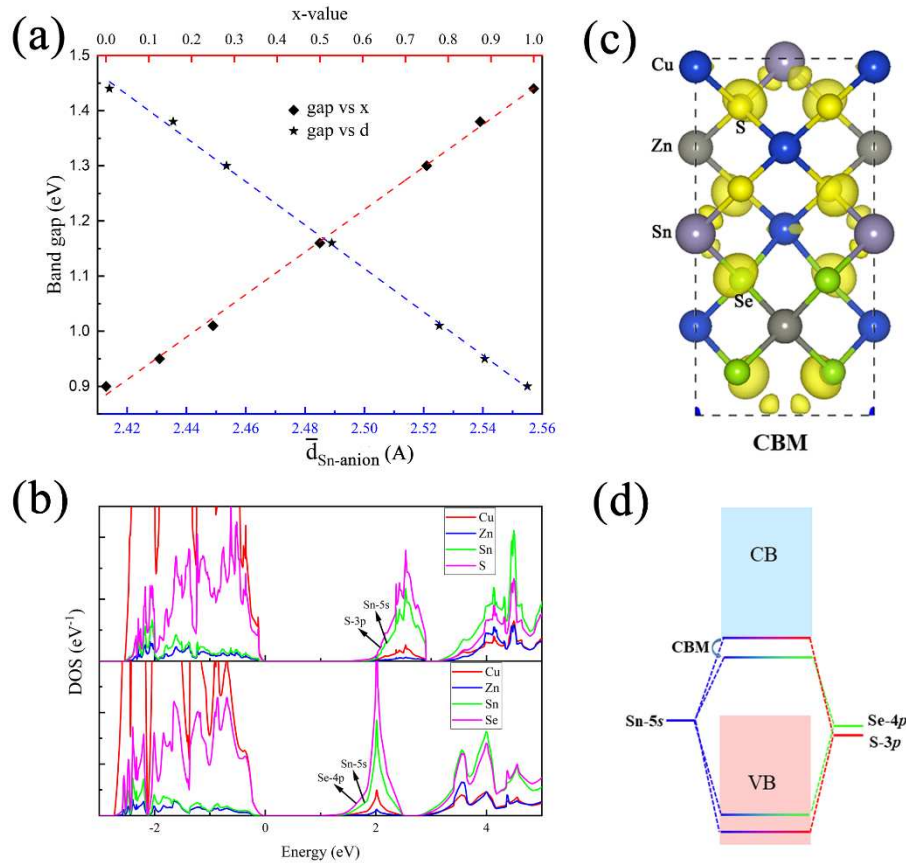
Figure 3. (a) Variation of the band gap in $CZT(S_xSe_{1-x})_4$ with both x and the average Sn-anion bond length as defined in Eq. (1). The dashed lines are linear fits. (b) Calculated Densities of states (DOS) in pure CZTS (top) and CZTSe (bottom). (c) Charge density isosurface corresponding to an electron in the conduction band minimum when x equals to 0.5 in $CZT(S_xSe_{1-x})_4$. (d) Schematic showing how introduction of Se lowers the conduction band minimum through reducing the antibonding interaction between Sn-5s and anion 3p states.

In the results above first principles calculations have been presented and compared against experimental data in order to both validate theoretical approximations and interpret results. However, one should be aware that there are a number of factors that can make direct quantitative comparisons

challenging. Firstly, the theoretical calculations consider perfectly stoichiometric $Cu_2ZnSn(S_xSe_{1-x})_4$ with only the ratio of anions permitted to vary, whereas real samples are usually non-stoichiometric to some degree (as shown in Table S5-S6 in SI). Secondly, real materials with mixed anion compositions are likely to exhibit significant anion disorder with local variations in the anion ratio throughout the sample. On the other hand, the theoretical models employ periodic supercells therefore true disorder is not captured which may affect predicted properties. The theoretical models also do not consider cation disorder which is likely to be present in real materials. However, despite these caveats the calculated lattice constants and band gaps, especially by HSE06 functional, are still very close to previous (both experimental and theoretical) results. The trends in the lattice constants, bond lengths and band gaps with varying mixing parameter x are also in very good agreement. Considering that there are also subtle differences in the experimental and theoretical definitions of some of these quantities (e.g. for bond length extraction via Rietveld refinement Sn atoms are assumed to be fixed at the high symmetry positions) the semi-quantitative agreement we find can be considered very good.

In summary, this work clarifies the sensitivity of the band gap to the Sn-anion bond length in mixed phases of CZTS and CZTSe. We also show that for accurate calculation of structural and electronic properties, it is essential to optimize at a level of theory that can reproduce the experimental Sn-anion bond lengths. The HSE06 hybrid functional is found to predict structures and band gaps for mixed anion phases [i.e. $Cu_2ZnSn(S_xSe_{1-x})_4$] in good agreement with experimental results. However, hybrid functional that involve non-local exchange contributions are computationally expensive which can be challenging for simulations requiring large supercells (such as those used to model the stability and electronic properties of point defects, surfaces or grain boundaries). For this reason, it is important to find computationally inexpensive methods for geometry optimization that can still capture the structure accurately. Our results show that geometry optimization with the MS2 meta-GGA functional followed by single point calculation of electronic properties using HSE06 gives very similar electronic properties to fully self-consistent HSE06 and therefore is a practical yet accurate approach for modelling complex defects in CZTSSe.

Density functional theory calculations: The density functional theory (DFT) calculations were performed using the projector augmented wave method to describe the interaction between ions and electrons, as implemented in the Vienna ab initio Simulation Package (VASP).[28-29] An accurate hybrid exchange-correlation functional HSE06[30] was used in all cases and to investigate the effect of different functionals we also employed the Perdew-Burke-Ernzerhof (PBE)[31] and MS2[32] functional for geometry optimization. An energy cutoff of 400 eV for the plane wave basis set was used and for the Brillouin-zone integration. The conventional cell (16 atoms in total) was used to model the mixed anion phase

$Cu_2ZnSn(S_xSe_{1-x})_4$, which contains 8 anion sites and we used a $7 \times 7 \times 3$ Monkhorst-Pack k-point mesh throughout all calculations. The most stable anion configuration was determined for each x (more details are provided in the SI, Figure S2).

Experimental methods: The bulk crystallised CZTSSe samples, 'Crystal' in Figure 2, were fabricated via solution growth from pre-synthesised CZTSSe dissolved in a molten NaCl-KCl mixture within a sealed quartz ampoule, for which the full details may be found in ref. 27. These samples were fabricated in increments of x of 0.1, with stoichiometric proportions of metals to S/Se selected through weighing of elemental powders. Samples were finely ground, and analysed with powder x-ray diffraction. Lattice parameters and atomic positions for S and Se were estimated from the diffraction patterns using Rietveld refinement (full measurement and refinement procedure also outlined in ref. 27). Refinement assumed that Sn atoms occupied fixed positions in the unit cell, while S and Se sites were treated as identical to one another. Partial Cu-Zn disorder was expected in all samples produced by this method.

The thin films, 'Thin film' in Fig.2, were synthesised via spray pyrolysis, in order to determine the band gap values for different values of x. The method consisted of dissolving precursors of copper chloride dihydrate ($CuCl_2$), zinc chloride dihydrate ($ZnCl_2$), tin (II) chloride dihydrate ($Cl_2H_4O_2Sn$), and thiourea (CH_4N_2S), into 25 ml of dimethyl sulphoxide (DMSO) and were then subsequently mixed with a magnetic stirrer until the solution was transparent and the precursors were fully dissolved (typically taking 5 minutes). The purity of the precursors purchased from Sigma Aldrich, were at least 99.5 % or higher and the sterilising procedure for the relevant equipment included cleaning with 5 % diluted lab detergent, followed by acetone, isopropanol, and finally de-ionised water.

The substrates used for optical measurements were fluorine-doped tin oxide (FTO), TEC 15 SLG glass. These substrates were cut to approx. 10 x 10 mm and placed on a hot plate for 1 minute at 320 $^\circ$C. Using an Iwata eclipse airbrush, a layer of solution was sprayed approx. 45 $^\circ$ from the substrate normal and left to heat for a further 1 minute, this was then repeated 2 more times to produce a thin film of thickness 0.48 $\pm$ 0.10 μm, as determined by cross-sectional SEM using the JSM-6610, using a 20 keV electron beam. Techinstro 500 nm molybdenum coated glass substrates and 5 layers of solution were used for all other characterisation techniques.

A closed space sublimation (CSS) method was adopted for further sulphurisation or selenisation treatments under a nitrogen gas atmosphere at a pressure of 300 Torr, at 520 $^\circ$C for 20 mins. The powder masses of sulphur and selenium were controlled, ranging from 40 – 100 mg, where the composition values were then verified by Energy Dispersive X-ray Spectroscopy (EDX), shown in Table S5 in SI.

Thin film XRD was measured with a Rigaku Smartlab Diffractometer, using a monochromatic Cu Kα1 x-ray source (λ = 1.541 Å). The thin film diffraction pattern is shown in Figure S3 in SI. The optical absorption study of the thin films was performed using the SolidSpec-3700 UV-vis-IR

spectrometer, within a wavelength range of 300 - 1500 nm. The resolution of the spectrometer was $\pm$ 0.1 nm, with an accuracy of $\pm$ 0.2 nm in the UV-vis range and $\pm$ 0.8 nm in the NIR range. The corresponding Tauc plots for the thin films are shown in Figure S4 in SI.

Supporting Information

Lattice, bond length and band gap information of the mixed phase by three different simulated functionals (PBE, MS2, HSE06) and experimental measurements, optimized possible initial configurations in the mixed phase, XRD pattern and Tauc plots for the thin film samples.

Acknowledgements

(1) Larramona, G.; Bourdais, S.; Jacob, A.; Choné, C.; Muto, T.; Cuccaro, Y.; Delatouche, B.; Moisan, C.; Péré, D.; Dennler, G. 8.6% Efficient CZTSSe Solar Cells Sprayed from Water–Ethanol CZTS Colloidal Solutions. *J. Phys. Chem. Lett.* **2014,** *5*, 3763-3767.

(2) Ravindiran, M.; Praveenkumar, C. Status Review and the Future Prospects of CZTS Based Solar Cell – A Novel Approach on the Device Structure and Material Modeling for CZTS Based Photovoltaic Device. *Renew. Sustainable Energy Rev.* **2018,** *94*, 317-329.

(3) Haddout, A.; Raidou, A.; Fahoume, M. A Review on the Numerical Modeling of CdS/CZTS-Based Solar Cells. *Applied Physics A* **2019,** *125*, 124.

(4) Guijarro, N.; Prévot, M. S.; Sivula, K. Enhancing the Charge Separation in Nanocrystalline Cu_2ZnSnS_4 Photocathodes for Photoelectrochemical Application: The Role of Surface Modifications. *J. Phys. Chem. Lett.* **2014,** *5*, 3902-3908.

(5) Yu, X.; Wang, D.; Liu, J.; Luo, Z.; Du, R.; Liu, L.-M.; Zhang, G.; Zhang, Y.; Cabot, A. Cu_2ZnSnS_4 Nanocrystals as Highly Active and Stable Electrocatalysts for the Oxygen Reduction Reaction. *J. Phys. Chem. C* **2016,** *120*, 24265-24270.

(6) Katagiri, H.; Sasaguchi, N.; Hando, S.; Hoshino, S.; Ohashi, J.; Yokota, T. Preparation and Evaluation of Cu_2ZnSnS_4 Thin Films by Sulfurization of E—B Evaporated Precursors. *Sol. Energy Mater. Sol. Cells* **1997,** *49*, 407-414.

(7) Green, M. A.; Dunlop, E. D.; Hohl-Ebinger, J.; Yoshita, M.; Kopidakis, N.; Hao, X. Solar Cell Efficiency Tables (Version 56). *Progress in Photovoltaics: Research and Applications* **2020,** *28*, 629-638.

(8) Kumar, M.; Dubey, A.; Adhikari, N.; Venkatesan, S.; Qiao, Q. Strategic Review of Secondary Phases, Defects and Defect-Complexes in Kesterite CZTS–Se Solar Cells. *Energy Environ. Sci.* **2015,** *8*, 3134-3159.

(9) Walsh, A.; Chen, S.; Wei, S.-H.; Gong, X.-G. Kesterite Thin-Film Solar Cells: Advances in Materials Modelling of Cu_2ZnSnS_4. *Adv. Energy Mater.* **2012,** *2*, 400-409.

(10) Chen, S.; Yang, J.-H.; Gong, X. G.; Walsh, A.; Wei, S.-H. Intrinsic Point Defects and Complexes in the Quaternary Kesterite Semiconductor Cu_2ZnSnS_4. *Phys. Rev. B* **2010,** *81*, 245204.

(11) Kim, S.; Park, J.-S.; Walsh, A. Identification of Killer Defects in Kesterite Thin-Film Solar Cells. *ACS Energy Lett.* **2018,** *3*, 496-500.

(12) Li, S.-y.; Zamulko, S.; Persson, C.; Ross, N.; Larsen, J. K.; Platzer-Björkman, C. Optical Properties of $Cu_2ZnSn(S_xSe_{1-x})_4$ Solar Absorbers: Spectroscopic Ellipsometry and Ab Initio Calculations. *Appl. Phys. Lett.* **2017,** *110*, 021905.

(13) Gang, M. G.; Shin, S. W.; Suryawanshi, M. P.; Ghorpade, U. V.; Song, Z.; Jang, J. S.; Yun, J. H.; Cheong, H.; Yan, Y.; Kim, J. H. Band Tail Engineering in Kesterite $Cu_2ZnSn(S,Se)_4$ Thin-Film Solar Cells with 11.8% Efficiency. *J. Phys. Chem. Lett.* **2018,** *9*, 4555-4561.

(14) Yang, K.-J.; Kim, S.; Kim, S.-Y.; Ahn, K.; Son, D.-H.; Kim, S.-H.; Lee, S.-J.; Kim, Y.-I.; Park, S.-N.; Sung, S.-J.; *et al*. Flexible $Cu_2ZnSn(S,Se)_4$ Solar Cells with over 10% Efficiency and Methods of Enlarging the Cell Area. *Nat. Commun.* **2019,** *10*, 2959.

(15) Yang, K.-J.; Son, D.-H.; Sung, S.-J.; Sim, J.-H.; Kim, Y.-I.; Park, S.-N.; Jeon, D.-H.; Kim, J.; Hwang, D.-K.; Jeon, C.-W.; *et al*. A Band-Gap-Graded CZTSSe Solar Cell with 12.3% Efficiency. *J. Mater. Chem. A* **2016,** *4*, 10151-10158.

(16) Omrani, M. K.; Minbashi, M.; Memarian, N.; Kim, D.-H. Improve the Performance of CZTSSe Solar Cells by Applying a SnS BSF Layer. *Solid-State Electron.* **2018,** *141*, 50-57.

(17) Min, J.-H.; Jeong, W.-L.; Kim, K.; Lee, J.-S.; Kim, K.-P.; Kim, J.; Gang, M. G.; Hong, C. W.; Kim, J. H.; Lee, D.-S. Flexible High-Efficiency CZTSSe Solar Cells on Diverse Flexible Substrates Via an Adhesive-Bonding Transfer Method. *ACS Appl. Mater. Interfaces* **2020,** *12*, 8189-8197.

(18) Azzouzi, M.; Cabas-Vidani, A.; Haass, S. G.; Röhr, J. A.; Romanyuk, Y. E.; Tiwari, A. N.; Nelson, J. Analysis of the Voltage Losses in CZTSSe Solar Cells of Varying Sn Content. *J. Phys. Chem. Lett.* **2019,** *10*, 2829-2835.

(19) Li, X.; Qian, X.; Cao, Y.-Q.; Cao, Z.-Y.; Liu, X.-J.; Zhu, L.; Li, A.-D.; Liu, W.-C.; Wu, D. A Facile and Low-Cost Synthesis of $Cu_2ZnSn(S_xSe_{1-x})_4$ Nanocrystals with Tunable Composition and Optical Band Gap. *Mater. Lett.* **2015,** *150*, 12-15.

(20) Mohammadnejad, S.; Baghban Parashkouh, A. CZTSSe Solar Cell Efficiency Improvement Using a New Band-Gap Grading Model in Absorber Layer. *Applied Physics A* **2017,** *123*, 758.

(21) Chen, S.; Walsh, A.; Yang, J.-H.; Gong, X. G.; Sun, L.; Yang, P.-X.; Chu, J.-H.; Wei, S.-H. Compositional Dependence of Structural and Electronic Properties of $Cu_2ZnSn(S,Se)_4$ Alloys for Thin Film Solar Cells. *Phys. Rev. B* **2011,** *83*, 125201.

(22) Jyothirmai, M. V.; Saini, H.; Park, N.; Thapa, R. Screening of Suitable Cationic Dopants for Solar Absorber Material CZTS/Se: A First Principles Study. *Sci. Rep.* **2019,** *9*, 15983.

(23) Nagoya, A.; Asahi, R.; Kresse, G. First-Principles Study of Cu_2ZnSnS_4 and the Related Band Offsets for Photovoltaic Applications. *J. Phys.: Condens. Matter* **2011,** *23*, 404203.

(24) Chen, S.; Gong, X. G.; Walsh, A.; Wei, S.-H. Defect Physics of the Kesterite Thin-Film Solar Cell Absorber Cu_2ZnSnS_4. *Appl. Phys. Lett.* **2010,** *96*, 021902.

(25) Zhong, G.; Tse, K.; Zhang, Y.; Li, X.; Huang, L.; Yang, C.; Zhu, J.; Zeng, Z.; Zhang, Z.; Xiao, X. Induced Effects by the Substitution of Zn in Cu_2ZnSnX_4 (X=S and Se). *Thin Solid Films* **2016,** *603*, 224-229.

(26) Park, J.-S.; Kim, S.; Hood, S. N.; Walsh, A. Open-Circuit Voltage Deficit in Cu_2ZnSnS_4 Solar Cells by Interface Bandgap Narrowing. *Appl. Phys. Lett.* **2018,** *113*, 212103.

(27) Hobson, T. D. C.; Hutter, O. S.; Fleck, N.; Daniels, L. M.; Major, J. D.; Ng, T. M.; Durose, K. Vegard Relation and Raman Band Reference Data Generated from Bulk Crystals of Kesterite-Phase Composition Series $Cu_2ZnSnS_{4x}Se_{4-4x}$ (CZTSSe, $0 \leq X \leq 1$). *Cryst. Growth Des.* **2020,** *20*, 2164-2173.

(28) Blochl, P. E. Projector Augmented-Wave Method. *Phys. Rev. B* **1994,** *50*, 17953-17979.

(29) Kresse, G. From Ultrasoft Pseudopotentials to the Projector Augmented-Wave Method. *Phys. Rev. B* **1999,** *59*, 1758-1775.

(30) Heyd, J.; Scuseria, G. E.; Ernzerhof, M. Erratum: "Hybrid Functionals Based on a Screened Coulomb Potential" [J. Chem. Phys. 118, 8207 (2003)]. *J. Chem. Phys.* **2006,** *124*, 219906.

(31) Perdew, J. P.; Burke, K.; Ernzerhof, M. Generalized Gradient Approximation Made Simple. *Phys. Rev. Lett.* **1996,** *77*, 3865-3868.

(32) Sun, J.; Xiao, B.; Fang, Y.; Haunschild, R.; Hao, P.; Ruzsinszky, A.; Csonka, G. I.; Scuseria, G. E.; Perdew, J. P. Density Functionals That Recognize Covalent, Metallic, and Weak Bonds. *Phys. Rev. Lett.* **2013,** *111*, 106401.